Geometrically induced broadening for phonon blocking at low temperatures

Kiminori Hattori and Yohei Nakamura

Department of Systems Innovation, Graduate School of Engineering Science, Osaka University, Toyonaka, Osaka 560-8531, Japan

Because of the presence of robust massless modes with no excitation gap, the heat current carried by phonons tends to survive at low temperatures even when scattering mechanisms are incorporated into the system. This becomes a fundamental obstacle to thermoelectric applications at low temperatures. In this study, we investigate the effect of energy broadening on phonon transport in mesoscopic systems coupled to leads or probes in various geometries using a nonequilibrium Green's function formalism. An analytic theory derived from a minimal model consisting of a harmonic chain shows that geometrically induced broadening sizably suppresses low-temperature phonon transport. It is also demonstrated from numerical calculations that this scheme for phonon blocking is viable for realistic systems in higher dimensions.

I. INTRODUCTION

In recent years, the heat flux carried by phonons in mesoscopic systems has garnered a great deal of attention in condensed matter physics [1,2]. In such situations, some conventional physical concepts break down. For instance, Fourier's law that relates heat current and temperature gradient is no longer valid, and thereby thermal conductivity is ill-defined. In particular, it is easily seen from the Landauer formula for ballistic phonon transport that at low temperatures, the thermal conductance G_{th} becomes material independent and quantized in integer multiples of the thermal conductance quantum defined by $G_0 = (\pi k_{\text{B}})^2 T/3h$, where T denotes the temperature [3–5]. This is parallel to the electric conductance G_{el}, which is quantized in units of e^2/h for metallic quantum wires [6,7]. These two conductance quanta are interrelated by the standard Lorentz number and satisfy the Wiedemann-Franz law, indicating that G_0 is universal for phonons and electrons despite the difference in their particle statistics [3,8]. The experimental observation of universal thermal conductance across a dielectric nanoscale junction is a hallmark of ballistic phonon transport in the mesoscopic regime [8]. In the ballistic transport regime, G_{th} becomes independent of transport length. This feature has been observed in experiments for semiconducting nanowires, even at room temperature [2,9,10].

Currently, it is becoming increasingly important to understand and thereby manage thermal transport at the nanoscale. This is not only due to the purely physical interest in this topic, but also because of the technological applicability to thermoelectrics that allows mutual conversion between thermal energy and electric energy [1,2,11]. The conversion efficiency is measured by the dimensionless figure of merit $ZT = G_{\text{el}}S^2T/G_{\text{th}}$, where S denotes the thermopower or Seebeck coefficient. As seen in the above expression, a lower G_{th} is favorable to thermoelectric applications. In semiconducting systems available to thermoelectrics, $G_{\text{th}} = G_{\text{th}}^{(e)} + G_{\text{th}}^{(p)}$ is normally dominated by the phononic contribution $G_{\text{th}}^{(p)}$ rather than its electronic counterpart $G_{\text{th}}^{(e)}$. Thus an important issue in this field constitutes how to suppress phonon transport. To this end, several approaches have been investigated so far. The suggested strategies consist mainly of adding scattering mechanisms due to alloying [12–14] or defects [15,16], surface roughness [2,17–21] or decoration [22], and geometric deformation of thermal pathways [23–31]. However, these effects are often limited because of residual quantum channels stemming from robust massless modes with no excitation gap, by which low-temperature phonon transport remains intact [2,15–19,21,22,26–31].

Our approach to this issue is as follows. In practice, a mesoscopic system such as a nanojunction is not isolated but is coupled to its environment. In terms of the quantum Langevin equation, macroscopic reservoirs are sources of noise and dissipation. The fluctuation-dissipation theorem relates the noise-noise correlation to the linewidth induced in the system [2,32]. The resulting energy broadening, which depends on the geometric configuration of the system and the reservoir, substantially affects the thermal conductance across the system through the self-energy due to the reservoir. The purpose of this paper is to show that this connection is exploitable for phonon blocking at low temperatures.

Partly, the present study is analogous to some of the previous ones [23–25], where phonon transport across an abrupt junction between a nanowire and an infinitely large bulk reservoir is analyzed in accordance with the scattering theory. In this study, we reformulate the physics of phonon blocking in terms of the broadening mechanism. Moreover, we analyze the effects of geometry and disorder in a lattice model on an equal footing. The latter may be an important issue when addressing phonon transport in realistic systems, which are not perfectly ordered but usually contain a number of defects.

Prior to this discussion, it may be appropriate to summarize our methodology. This study is based on the nonequilibrium Green's function formalism [16,33,34] as well as the quantum Langevin equation approach [2,32], which give a thoroughly rigorous expression for heat currents carried by phonons in noninteracting quantum systems coupled to heat reservoirs held at different temperatures. The systems are described by harmonic lattice Hamiltonians. To capture generic features

in thermal transport, we focus on simple representative lattice models without assuming specific materials. We neglect phonon-phonon interactions due to lattice anharmonicity. Thus thermal transport is evaluated without approximation validly in the low-temperature regime where nonlinear quantum effects are immaterial [35–38].

The paper is organized as follows. To begin with, in Sec. II, we summarize the theoretical formulas including lattice Hamiltonians used in this study. To be self-contained, in Sec. III, we briefly explain phonon transport in the presence of disorder. At low temperatures, phonon transport is dominated by gapless modes that are immune to disorder by virtue of the acoustic sum rule. The robust massless modes tend to prohibit total thermal insulation. In Sec. IV, we show that this fundamental difficulty is circumvented by connecting the system to leads or probes of different geometries. Introducing a minimal model, an analytic theory is derived for phonon blocking in terms of the linewidth correlated to geometry. In Sec. V, numerical results are discussed for more realistic models in the absence or the presence of disorder, demonstrating that phonon blocking is realizable over a broad temperature range with the assistance of disorder. Finally, Sec. VI provides a summary.

II. THEORETICAL FORMULATION

This section summarizes the lattice Hamiltonians and the theoretical formulas used for analyzing thermal transport. Henceforth, we simplify the notation $G_{\text{th}}^{(\text{p})}$ into G for brevity since we consider the phononic contribution only. The Hamiltonian describing an isotropic elastic continuum is given by

$$H = \frac{1}{2} \int d\mathbf{r}[\rho \dot{\mathbf{q}} \cdot \dot{\mathbf{q}} - (\lambda + \mu)\mathbf{q} \cdot \nabla \nabla \cdot \mathbf{q} - \mu \mathbf{q} \cdot \nabla^2 \mathbf{q}], \quad (1)$$

where $\rho(\mathbf{r})$ is the mass density, λ and μ are the Lamé's constants, and $\mathbf{q}(\mathbf{r})$ is the vector displacement field at position $\mathbf{r}$. In the following, we assume $\lambda = \mu$ for simplicity. The finite difference method is used to map this Hamiltonian onto a cubic lattice with lattice spacing a. The result is simply formulated as

$$H = \frac{1}{2}(\dot{q}^t M \dot{q} + q^t K q), \quad (2)$$

in terms of the column vector q consisting of vector displacements $(q_\mathbf{r}^x, q_\mathbf{r}^y, q_\mathbf{r}^z)$ at all lattice points $\mathbf{r}$. The mass matrix and force-constant matrix are explicitly expressed as $M_{\mathbf{rr'}}^{ij} = m_\mathbf{r} \delta_{\mathbf{rr'}} \delta_{ij}$ and

$$K^{ij} = \bar{K} \left[\left(\Delta^i + \sum_{k \neq i} \frac{\Delta^{i+k} + \Delta^{i-k}}{2} \right) \delta_{ij} \right.$$
$$\left. + \frac{\Delta^{i+j} - \Delta^{i-j}}{2}(1 - \delta_{ij}) \right], \quad (3)$$

respectively. Here,

$$m_\mathbf{r} = \rho(\mathbf{r})a^3,$$
$$\bar{K} = \mu a,$$
$$\Delta_{\mathbf{rr'}}^i = 2\delta_{\mathbf{rr'}} - \delta_{\mathbf{r},\mathbf{r'}+\mathbf{a}_i} - \delta_{\mathbf{r},\mathbf{r'}-\mathbf{a}_i},$$
$$\Delta_{\mathbf{rr'}}^{i \pm j} = 2\delta_{\mathbf{rr'}} - \delta_{\mathbf{r},\mathbf{r'}+(\mathbf{a}_i \pm \mathbf{a}_j)} - \delta_{\mathbf{r},\mathbf{r'}-(\mathbf{a}_i \pm \mathbf{a}_j)},$$

and $\mathbf{a}_i$ denotes the unit lattice vector in the direction $i \in \{x, y, z\}$. It is easy to obtain the lattice expressions reduced in lower dimensions. For instance, $K = \bar{K}(\Delta^x + \Delta^y)$ for out-of-plane displacements of atoms in a square lattice in the xy plane (shear horizontal mode). This corresponds to the scalar model of two-dimensional (2D) harmonic lattice. Analogously, $K = \bar{K}\Delta^x$ for a shear mode in a 1D harmonic chain along x.

In multiterminal geometry, the retarded Green's function is generally written as

$$g = \frac{1}{\varepsilon^2 - D - \sum_\alpha \Sigma_\alpha}, \quad (4)$$

where $D = \hbar^2 M^{-1/2} K M^{-1/2}$ is the dynamical matrix, and Σ_α denotes the retarded self-energy due to a lead α. Following the nonequilibrium Green's function formalism [16,33,34] or equivalently the quantum Langevin equation approach [2,32], the heat current flowing in lead α is described by the linearized Landauer-Büttiker formula

$$J_\alpha = \sum_\beta G_{\alpha\beta}(T_\alpha - T_\beta) \quad (5)$$

for a small enough temperature difference $T_\alpha - T_\beta$. The thermal conductance between leads α and β is expressed as

$$G_{\alpha\beta} = \frac{1}{h} \int_0^\infty d\varepsilon \frac{\partial f}{\partial T} \varepsilon \mathcal{T}_{\alpha\beta}, \quad (6)$$

where $\mathcal{T}_{\alpha\beta} = \text{Tr } \gamma_\alpha g \gamma_\beta g^*$ is the transmission coefficient, $\gamma_\alpha = -2 \text{Im } \Sigma_\alpha$ is the linewidth function, and $f = (e^{\varepsilon/k_\text{B}T} - 1)^{-1}$ is the Bose function for phonons. The thermal conductance quantum G_0 corresponds to G for $\mathcal{T} = 1$.

III. MASSLESS MODES PROTECTED BY THE ACOUSTIC SUM RULE

As mentioned in Sec. I, a simple way to reduce thermal conductance is to disorder the system that transports phonons. To demonstrate this, we employ scalar 2D models, into which isotropic disorder and surface roughness are incorporated. In the calculation, the former is modeled by random masses deviating from the mean m by $\delta m = \pm 0.1m$ with equal probability. For the latter, we consider a multilayer randomly stacked with two segments of equal length $l = 5a$ and different widths $w = 10a$ and $12a$, where the fluctuations $\delta w = \pm a$ occur with a probability of $1/2$. See, the insets in Fig. 1 for reference. Note that disordering is thoroughly implemented in the lattice model (unlike the relaxation time approximation in the Boltzmann equation approach). In this sense, the numerical results shown here are exact. Figure 1 summarizes the transmission coefficient $\mathcal{T}$ and the thermal conductance G derived from Eq. (6). As seen in this figure, disorder reduces $\mathcal{T}$ appreciably over a wide energy range. The reduced $\mathcal{T}$ is naturally reflected in G. At high temperatures, G monotonically diminishes as the system length L_x increases, signaling diffusive phonon transport in the presence of disorder. On the other hand, $\mathcal{T}$ remains unaffected at low energies. Correspondingly, the low-temperature G stays quantized at G_0 regardless of disorder.

These observations do not contradict the probability of phonon scattering caused by each type of disorder. From perturbation theory, the reciprocal phonon lifetime is evaluated for mass disorder to be $\tau^{-1} \propto \frac{\langle \delta m^2 \rangle}{m^2} \varepsilon^2 N(\varepsilon)$ to the lowest
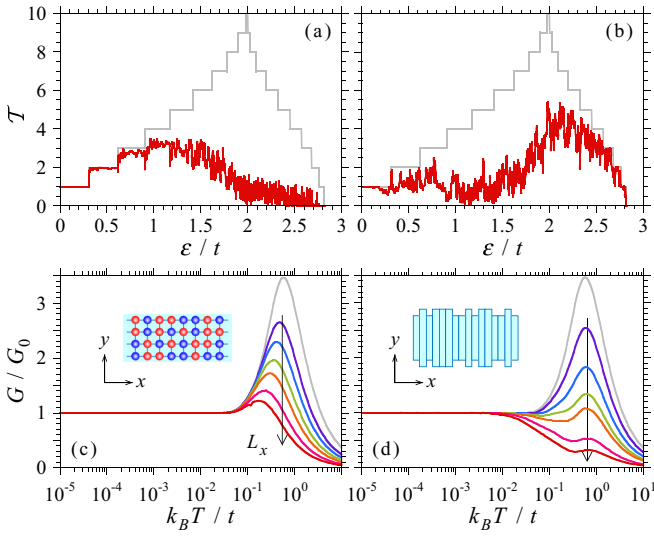
FIG. 1. Effects of disorder on thermal transport. [(a) and (b)] Transmission coefficient $\mathcal{T}$ as a function of energy ε and [(c) and (d)] thermal conductance G as a function of temperature T calculated for scalar 2D models with [(a) and (c)] mass fluctuations $\delta m = \pm 0.1m$ and [(b) and (d)] width fluctuations between $w = 10a$ and $12a$. Each plot corresponds to a single realization of disorder. The system length is set to be $L_x = 100a$ in (a) and (b), while L_x are varied as $20a$, $50a$, $100a$, $200a$, $500a$, and $1000a$ in (c) and (d). The system width is chosen to be $L_y = 10a$ for (a) and (c). The gray line in each figure displays the numerical result in the absence of disorder as a reference. Note that in this case, phonon transport is ballistic so that both $\mathcal{T}$ and G are independent of L_x. Insets in (c) and (d) are schematics for the models used in the calculations.

nonvanishing order in δm, where the angular brackets stand for statistical average, and $N(\varepsilon)$ denotes the phonon density of states [39,40]. This implies that mass disorder is irrelevant to low-energy phonon transport. The probability of specular reflection at a Gaussian rough surface amounts to $\exp(-k^2\langle \delta w^2 \rangle)$, where k represents the phonon wave number [2,35]. In view of this, surface roughness is essentially negligible in the long-wavelength limit. Phonon-phonon interactions stemming from lattice anharmonicity are neglected in the present study. However, it may be worth noting that the relevant scattering rate vanishes in the low-energy or low-temperature limit [35–38], suggesting that phonon transport is intrinsically stable at low temperatures even in interacting systems. This conjecture is corroborated by numerical calculations for nanojunction atomic systems with anharmonic interactions based on diagrammatic perturbation theory [36].

More generically, the robustness of low-temperature phonon transport is accountable for in terms of the equation of motion $m_{\mathbf{r}}\ddot{q}_{\mathbf{r}} + \sum_{\mathbf{r}'} K_{\mathbf{r}\mathbf{r}'} q_{\mathbf{r}'} = 0$. The force-constant matrix generally obeys the acoustic sum rule such that

$$\sum_{\mathbf{r}'} K_{\mathbf{r}\mathbf{r}'} = 0, \tag{7}$$

because of the conservation of total linear momentum or equivalently the invariance of the equation of motion under rigid translations. This constraint ensures that there exist massless modes with no excitation gap. In other words, gapless

modes always emerge in momentum-conserving systems. By definition, the low-temperature conductance is expressed as $\lim_{T\to 0} G/G_0 = \lim_{\varepsilon\to 0} \mathcal{T}$ so that G/G_0 represents the number of propagating massless modes at low temperatures. This is why low-temperature transport is insensitive to disorder. The conclusion is not altered even for vector displacements in a 3D lattice. An analogous argument is applicable to elastic waves in 3D. It is well known that stress-free boundary conditions at free surfaces allow massless modes to occur in a finite elastic body. In terms of the equation of motion $\rho \ddot{q}^i = \sum_j \partial_j T^{ij}$, the stress tensor T^{ij} represents a flux of the i component of momentum across the surface normal to j. Thus the stress-free boundary enclosing an elastic system naturally leads to total momentum conservation in terms of the divergence theorem.

IV. PHONON BLOCKING DUE TO BROADENING

Robust massless modes tend to set a fundamental limit to suppressing thermal transport in the mesoscopic regime. This may bottleneck low-temperature thermoelectrics such as cryogenic solid-state coolers, which are beneficial for nanoscale thermometers or radiation detectors, superconducting microelectronics, and probably solid-state quantum computation [11,41]. A higher ZT as a result of a lower G is suitable for thermoelectric refrigeration. This can be shown from the lowest attainable temperature, expressed as $T_c = T_h/\sqrt{1+ZT}$, where T_c and T_h denote cold and hot junction temperatures, respectively. In what follows, we analyze the energy broadening induced by leads or probes attached to the system for blocking low-temperature phonon transport.

For simplicity, we assume a 1D harmonic chain as a minimal model, from which an analytic formulation is derived. The retarded Green's function of a linear chain consisting of n lattice sites is analyzable in the iterative manner formulated as [2,33]

$$g_{nn} = \left(g_0^{-1} - t^4 g_{n-1,n-1}\right)^{-1}, \tag{8}$$

$$g_{1n} = -t^2 g_{1,n-1} g_{nn}. \tag{9}$$

Here, $g_{jj'}$ represents the matrix element of the Green's function between sites j and j', $t = \hbar\sqrt{\bar{K}/m}$ is the characteristic energy scale of the harmonic lattice, and $\bar{K}$ denotes the intersite force constant. For Si, $\bar{K}$ is evaluated to be $17\,\mathrm{N\,m^{-1}}$ [42], yielding an estimate $t \simeq 12$ meV. In Eq. (8), $g_0 = (\varepsilon^2 - bt^2)^{-1}$ refers to the Green's function of an isolated site, and b is an integer that reflects the acoustic sum rule. In a linear chain, each inner site couples to two nearest neighbors so that $b = 2$. For a semi-infinite chain, the surface Green's function obeys $g_{nn} = g_{n-1,n-1} \equiv g$. This leads to the quadratic Dyson equation $g = g_0(1 + t^4 g^2)$. The solution is found to be $g = -\lambda/t^2$ and $\lambda = \exp(2i\sin^{-1}z)$, where $z = \varepsilon/2t$. To evaluate heat flow, we consider a two-terminal system where a finite chain is connected to two semi-infinite leads serving as heat reservoirs at both ends. In this geometry, the Green's functions are computed by adding sites one by one to an isolated lead until reaching the opposite lead. For a finite chain in contact with a semi-infinite lead, one easily finds that $g_{11} = (g_0^{-1} - \Sigma) = g$ and thereby $g_{22} = \cdots = g_{nn} = g$,

where $\Sigma = -t^2\lambda$ is the retarded self-energy due to the lead. After coupling to the opposite lead, the end-site Green's function becomes $g_{nn} = (g^{-1} - \Sigma)^{-1} = -i\gamma^{-1}$, where $\gamma = -2\,\mathrm{Im}\,\Sigma$ is the linewidth function. Analogously, the intersite Green's function is derived to be $g_{1n} = \lambda^{n-1}g_{nn}$. In terms of the Landauer formula, the two-terminal transmission coefficient is given by $\mathcal{T} = \gamma^2|g_{1n}|^2 = 1$. This coincides with the well-known result deduced from analytic matrix inversion [2,34].

Armed with the recursive Green's function formalism, we next proceed to analyze a 1D chain in contact with a semi-infinite 2D lead of a finite width $W = Ma$. Unfortunately, there is no analytic formulation in 2D. Instead, numerically solving the relevant Dyson equation, it is found that the surface Green's function is approximately represented as $g_M = -\lambda_M/t^2$ with $\lambda_M = 1 + 2iMz$ in the $\varepsilon \to 0$ limit. This corresponds to the self-energy $\Sigma_M = -t^2\lambda_M$ and the linewidth $\gamma_M = M\gamma$, indicating that the imaginary part of the self-energy is augmented by coupling to the 2D lead while leaving the real part unchanged. For an asymmetric two-terminal system connected to 2D and 1D leads, it is easily shown that $g_{nn} = -2i\gamma_{M+1}^{-1}$ and $g_{1n} = \lambda_M^{n-1}g_{nn}$. From these results, we arrive at the transmission coefficient expressed as

$$\mathcal{T} = \gamma\gamma_M|g_{1n}|^2 = \frac{4M}{(M+1)^2}. \qquad (10)$$

The identical result is derived when replacing the 2D lead with a bunch of 1D leads. Equation (10) shows that the broadening induced by a sufficiently wide lead blocks low-temperature phonon transport since $\mathcal{T} \to 0$ as $M \to \infty$. These arguments are quantitatively confirmed in Fig. 2, where the numerical results for 2D-1D junctions are summarized. A similar behavior is seen in the previous study that considers the 1D wire coupled to bunched 1D leads [42]. Our theoretical treatment is further generalized by considering two 2D leads of different widths $W_{1,2} = M_{1,2}a$ attached to the system. In this case, we obtain

$$\mathcal{T} = \frac{4M_1M_2}{(M_1+M_2)^2}. \qquad (11)$$

Interestingly, this equation is structurally equivalent to the impedance-mismatch transmission $\mathcal{T} = 4Z_1Z_2/(Z_1+Z_2)^2$ between two homogeneous media with different acoustic impedances $Z_{1,2}$. In terms of Eq. (11), it is noticed that the geometric mismatch does not necessarily prevent thermal transport, since $\mathcal{T} = 1$ and then $G = G_0$ for $M_1 = M_2$. Thus asymmetric configurations are a prerequisite for phonon blocking in this scheme.

The source of broadening is not only current leads but also temperature probes attached to the system. Normally, the probe should be left floating, i.e., thermally isolated from the outside world except for the system. Local equilibration between the probe and the system is attained under the condition that no net thermal current flows between them. As a result, connecting the probe to the system introduces broadening without dissipation (i.e., no heat is dissipated in the probe). This is reminiscent of a fictitious probe strongly coupled to each site of a lattice system to mimic inelastic scattering [6,11,32]. Such a probe acts as a phase-breaking scatterer, whose strength is measured by its inducing linewidth. Thus it is expected that phonon transport is impeded not only by wide leads but also by wide probes. To
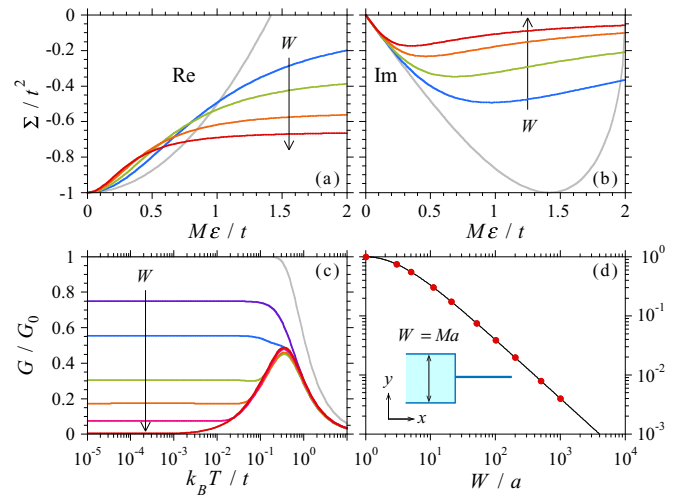
FIG. 2. Effects of 2D lead on 1D thermal transport. (a) Real and (b) imaginary parts of self-energy Σ_M due to 2D lead of width $W = Ma$ calculated as a function of scaled energy $M\varepsilon$, where M is varied as 3, 11, 101, and 1001. As found in the figures, Σ_M collapses onto the single function $-t^2(1 + iM\varepsilon/t)$ in the low-energy limit. (c) Thermal conductance G as a function of temperature T for 2D-1D junctions with $M=3, 5, 11, 21, 51$, and 1001. G exhibits a plateau at low enough temperatures. (d) $\lim_{T\to 0} G$ as a function of W. The gray lines in (a), (b), and (c) display the results for a normal 1D wire without geometric mismatch (for which $M = 1$) as references. The solid line in (d) represents the theoretical plot based on Eq. (10). Inset in (d) illustrates the geometry assumed for the analysis. Note that the central site on the right-side boundary of the 2D lead is coupled to the left end of the 1D chain.

show this, we consider a setup where a finite 1D chain situated between two 1D leads couples to a 2D probe locally at an inner site p of the chain. Note that $b = 3$ for the contact site p. The associated Green's functions are derived to be $g_{nn} = -2i\gamma_{M+2}^{-1}$, $g_{1p} = \lambda^{p-1}g_{nn}$ and $g_{1n} = \lambda_{M+1}^{n-p}\lambda^{p-1}g_{nn}$. Hence the lead-lead transmission is given by

$$\mathcal{T}_{1n} = \gamma^2|g_{1n}|^2 = \frac{4}{(M+2)^2}.$$

Similarly, the lead-probe transmission is expressed as

$$\mathcal{T}_{1p} = \gamma\gamma_M|g_{1p}|^2 = M\mathcal{T}_{1n}.$$

Note that both $\mathcal{T}_{1n}$ and $\mathcal{T}_{1p}$ are independent of probe position. The adiabatic condition leads to the two-terminal conductance $G = G_{1n} + G_{1p}G_{pn}/(G_{1p} + G_{pn})$, following the multiterminal Landauer formula. Reversing the iteration, it is easily found that $\mathcal{T}_{1p} = \mathcal{T}_{pn}$ and hence $G_{1p} = G_{pn}$. As a result, we reach the effective transmission

$$\mathcal{T} = \frac{2}{M+2}. \qquad (12)$$

Again, it is shown that $\mathcal{T} \to 0$ as $M \to \infty$. The analytic result is validated numerically as shown in Fig. 3. It is also confirmed numerically that low-temperature thermal conductance is unaffected by varying the number of contact sites for a given width of 2D probe (not shown). This implies that a large enough real probe connected to the system enables phonon blocking irrespective of the contact geometry.
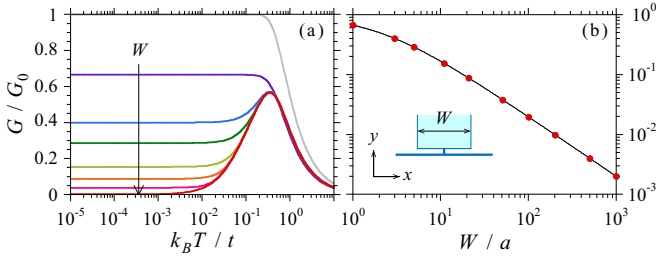
FIG. 3. Effects of 2D probe on 1D thermal transport. (a) Thermal conductance G as a function of temperature T for a 1D chain coupled to a 2D probe of width $W = Ma$, where M is varied as 1, 3, 5, 11, 21, 51, and 1001. G exhibits a plateau at low enough temperatures. (b) $\lim_{T \to 0} G$ as a function of W. The gray line in (a) displays the result for a normal 1D wire without probe as a reference. The solid line in (b) represents the theoretical plot based on Eq. (12). Inset in (b) illustrates the geometry assumed for the analysis. Note that the central site on the lower boundary of the 2D probe is in contact with an inner site of the 1D chain.

The broadening argument may become more transparent by considering the local density of states, defined by

$$N(x, \varepsilon) = -\frac{2\varepsilon}{\pi} \operatorname{Im} g_{jj}(\varepsilon)$$

per site, where $x = ja$ and $j = 1, 2, \ldots, n$. In view of Eq. (4), $N(x, \varepsilon)$ is reduced by the broadening due to leads or probes in contact with the system. This is analytically verifiable. From the on-site Green's function derived above, one finds $N(x, \varepsilon) = 2/(M + 1)\pi t$ for a 2D lead and $2/(M + 2)\pi t$ for a 2D probe in the low-energy limit. They become negligibly small for a sufficiently large M, compared to $1/\pi t$ for an infinitely long ordered 1D chain. The expected depletion in the low-energy regime is visible in Fig. 4, where numerical results are summarized for the 2D lead and the 2D probe. Although momentum-conserving systems always exhibit gapless spectra because of the acoustic sum rule, a vanishingly low density of states is realizable, which tends to suppress phonon propaga-
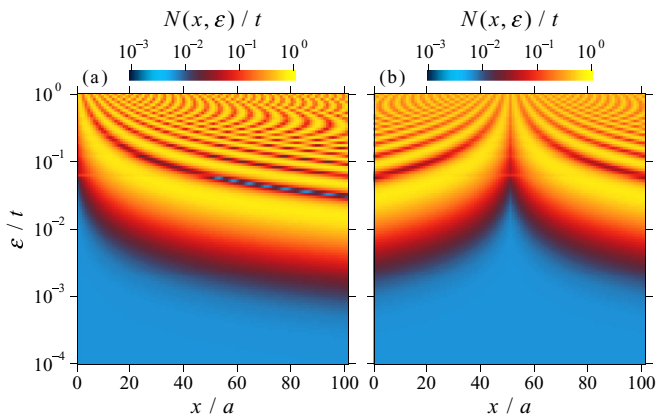
FIG. 4. Local density of states for (a) a 2D-1D junction and (b) a 1D chain coupled to a 2D probe. The geometries assumed in the calculations are identical to those for Figs. 2 and 3. The parameters are chosen to be $L_x = W = 101a$.
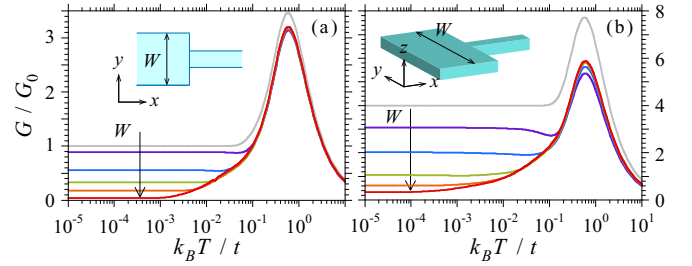
FIG. 5. Thermal conductance G as a function of temperature T for asymmetric (a) 2D-2D and (b) 3D-3D junctions. In (a), the system width is $L_y = 10a$, while the lead width $W = Ma$ is varied as M=20, 50, 100, 200, and 1000. In (b), the system width is $L_y = 4a$, while the lead width is varied as M=10, 20, 50, 100, and 200. In the 3D model, the same thickness $L_z = 4a$ is assumed for the system and the lead. The gray lines in (a) and (b) display the results for normal 2D and 3D wires without geometric mismatch as references, respectively. Insets are schematics for the models used in the calculations.

tion across the system. This provides an intuitive interpretation for the phonon blocking due to broadening.

V. NUMERICAL CALCULATION

The preceding section deals with the analytic theory for a 1D chain. In this section, we explore thermal transport in higher dimensions by using numerical calculations. As shown in Fig. 5(a), G/G_0 tends to vanish at low temperatures in asymmetric 2D-2D junctions when the lead width W increases sufficiently. Thermal transport in 3D is also numerically evaluated by employing the 3D vector model described in Sec. II. In this model, $G/G_0 = 4$ is observed for a uniform 3D rod at low temperatures. This represents contributions due to four intrinsic massless modes comprised of one extensional, one torsional, and two flexural modes. Low-temperature phonon transport via these fundamental modes is greatly suppressed in asymmetric 3D-3D junctions, as shown in Fig. 5(b). Previously, a similar but symmetric configuration has been argued for manipulating phonon transport [26,31,42]. As implied from our 1D lattice theory, in that case, perfect transmission of massless modes is sustained in the low-energy limit regardless of geometric mismatch. This reasonably accounts for the previous observations. It is also noted that the present results do not contradict the elastic-wave transmission vanishing at an abrupt junction between a nanowire and an infinitely large bulk reservoir at low frequencies [23–25]. In the elastic model, the quenched transmission is ascribed to interfacial scattering at the geometrically mismatched junction. In the lattice model, on the other hand, this is accounted for by geometry-dependent broadening.

Figure 6 displays the numerical results for 2D strips contacted by 2D probes at two transverse edges and 3D rods coupled to 3D probes at four side faces. In the 2D case, G/G_0 monotonically decreases with increasing the probe size W at low temperatures, and tends to vanish in the $W \to \infty$ limit. A similar reduction is observable in the 3D model, except a shallow valley appearing in temperature dependence. At the lower temperature side, G/G_0 ascends slightly from its minimum on lowering the temperature. It is verified from
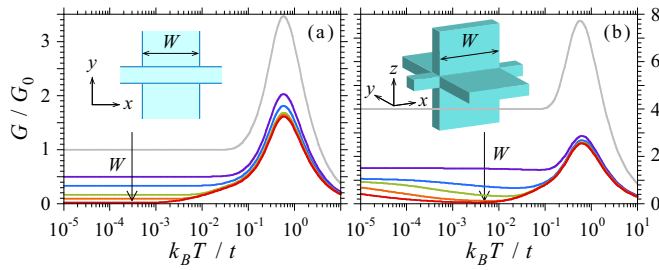
FIG. 6. Thermal conductance G as a function of temperature T for (a) 2D and (b) 3D wires coupled to side probes. In (a), the system width is $L_y = 10a$, while the probe width $W = Ma$ is varied as $M=10$, 20, 50, 100, and 500. In (b), the lateral dimensions are $L_y = L_z = 4a$ for the system and the probes, while the probe width is varied as $M=4$, 10, 20, 50, and 100. The gray lines in (a) and (b) display the results for normal 2D and 3D wires without probes as references, respectively. Insets are schematics for the models used in the calculations.

FIG. 7. Thermal conductance G as a function of temperature T for asymmetric 2D-2D junctions with (a) isotopic disorder and (b) surface roughness. The system length and the lead width are set to be $L_x = W = 1000a$. The other parameters are the same as those for Fig. 1. The gray lines in (a) and (b) display the result for a normal 2D wire without disorder and geometric mismatch as a reference. The results obtained with adding both disorder and geometric mismatch are shown by red lines in comparison with those only with disorder indicated by blue lines. Insets are schematics for the models used in the calculations.

additional calculations that in this region, thermal transport is dominated by longitudinal modes. The associated mechanism is unclear at the present stage of investigation. Nonetheless, it should be emphasized that the minimum G/G_0 is greatly reduced for a larger W. As expected, phonon transport is strongly suppressed even in a single-probe geometry if W is large enough. It is worth noting that in experiments, a macroscopically large substrate onto which a nanowire is mounted may act as such a probe to block phonon transport across the wire.

Thus far, we have assumed fully ballistic systems to elucidate phonon blocking at low temperatures. It is not necessarily evident that the present scheme is applicable to disordered systems, where phonon transport tends to be diffusive, as illustrated in Fig. 1. Figure 7 summarizes the numerical results for disordered systems to which a wide lead is attached. As seen in the figure, geometrically induced broadening and bulk or surface disorder suppress thermal transport separately in the low- and high-temperature regimes, respectively. This observation implies that phonon blocking is realizable by these two uncorrelated mechanisms over a wide temperature range. In the framework of perturbation theory, adding the nonlinear quantum effects due to lattice anharmonicity further suppresses

G at high temperatures [36]. In view of this, the present result amounts to its upper bound.

VI. SUMMARY

We have presented an analytic theory and numerical results for thermal transport across a system in contact with leads or probes of different geometries. The analytic formulas derived from a minimal model consisting of a 1D harmonic chain predict that low-temperature phonon transport via massless modes is substantially suppressed by geometrically engineered linewidth. Numerical calculations demonstrate that phonon blocking in this scheme is operative in more realistic systems in both ballistic and diffusive transport regimes. In particular, it is shown that adding the broadening mechanism to diffusive systems enables phonon blocking over a broad temperature range.

ACKNOWLEDGMENT

[1] Y. Dubi and M. D. Ventra, Rev. Mod. Phys. **83**, 131 (2011).

[2] *Thermal Transport in Low Dimensions*, edited by S. Lepri (Springer, Heidelberg, 2016).

[3] L. G. C. Rego and G. Kirczenow, Phys. Rev. Lett. **81**, 232 (1998).

[4] D. E. Angelescu, M. C. Cross, and M. L. Roukes, Superlattices and Microstruct. **23**, 673 (1998).

[5] M. P. Blencowe, Phys. Rev. B **59**, 4992 (1999).

[6] S. Datta, *Electronic Transport in Mesoscopic Systems* (Cambridge University Press, Cambridge, 1995).

[7] Y. Imry, *Introduction to Mesoscopic Physics* (Oxford University Press, New York, 2008).

[8] K. Schwab, E. A. Henriksen, J. M. Worlock, and M. L. Roukes, Nature (London) **404**, 974 (2000).

[9] T.-K. Hsiao, H.-K. Chang, S.-C. Liou, M.-W. Chu, S.-C. Lee, and C.-W. Chang, Nat. Nanotechnol. **8**, 534 (2013).

[10] B.-W. Huang, T.-K. Hsiao, K.-H. Lin, D.-W. Chiou, and C.-W. Chang, AIP Adv. **5**, 053202 (2015).

[11] G. Benenti, G. Casati, K. Saito, and R. S. Whitney, Phys. Rep. **694**, 1 (2017).

[12] C. Bera, N. Mingo, and S. Volz, Phys. Rev. Lett. **104**, 115502 (2010).

[13] J. Garg, N. Bonini, B. Kozinsky, and N. Marzari, Phys. Rev. Lett. **106**, 045901 (2011).

[14] G. Xie, Y. Guo, X. Wei, K. Zhang, L. Sun, J. Zhong, G. Zhang, and Y.-W. Zhang, Appl. Phys. Lett. **104**, 233901 (2014).

[15] K.-Q. Chen, W.-X. Li, W. Duan, Z. Shuai, and B.-L. Gu, Phys. Rev. B **72**, 045422 (2005).

[16] T. Yamamoto and K. Watanabe, Phys. Rev. Lett. **96**, 255503 (2006).

[17] A. Kambili, G. Fagas, V. I. Fal'ko, and C. J. Lambert, Phys. Rev. B **60**, 15593 (1999).

[18] D. H. Santamore and M. C. Cross, Phys. Rev. Lett. **87**, 115502 (2001).

[19] D. H. Santamore and M. C. Cross, Phys. Rev. B **63**, 184306 (2001).

[20] A. I. Hochbaum, R. Chen, R. D. Delgado, W. Liang, E. C. Garnett, M. Najarian, A. Majumdar, and P. Yang, Nature (London) **451**, 163 (2008).

[21] J. H. Oh, M. Shin, and M.-G. Jang, J. Appl. Phys. **111**, 044304 (2012).

[22] T. Markussen, A.-P. Jauho, and M. Brandbyge, Phys. Rev. Lett. **103**, 055502 (2009).

[23] M. C. Cross and R. Lifshitz, Phys. Rev. B **64**, 085324 (2001).

[24] C.-M. Chang and M. R. Geller, Phys. Rev. B **71**, 125304 (2005).

[25] W.-X. Li, T. Liu, and C. Liu, Appl. Phys. Lett. **89**, 163104 (2006).

[26] W.-X. Li, K.-Q. Chen, W. Duan, J. Wu, and B.-L. Gu, J. Phys. D **36**, 3027 (2003).

[27] W.-Q. Huang, K.-Q. Chen, Z. Shuai, L. Wang, W. Hu, and B. S. Zou, J. Appl. Phys. **98**, 093524 (2005).

[28] L.-M. Tang, L.-L. Wang, K.-Q. Chen, W.-Q. Huang, and B. S. Zou, Appl. Phys. Lett. **88**, 163505 (2006).

[29] X.-F. Peng, K.-Q. Chen, B. S. Zou, and Y. Zhang, Appl. Phys. Lett. **90**, 193502 (2007).

[30] L.-M. Tang, L. Wang, W.-Q. Huang, B. S. Zou, and K.-Q. Chen, J. Phys. D **40**, 1497 (2007).

[31] F. Xie, K.-Q. Chen, Y. G. Wang, and Y. Zhang, J. Appl. Phys. **103**, 084501 (2008).

[32] A. Dhar and D. Roy, J. Stat. Phys. **125**, 801 (2006).

[33] J.-S. Wang, J. Wang, and J. T. Lü, Eur. Phys. J. B **62**, 381 (2008).

[34] S. G. Das and A. Dhar, Eur. Phys. J. B **85**, 372 (2012).

[35] J. M. Ziman, *Electrons and Phonons* (Clarendon, Oxford, 1962).

[36] J.-S. Wang, J. Wang, and N. Zeng, Phys. Rev. B **74**, 033408 (2006).

[37] Y. Xu, J.-S. Wang, W. Duan, B.-L. Gu, and B. Li, Phys. Rev. B **78**, 224303 (2008).

[38] T. Feng, L. Lindsay, and X. Ruan, Phys. Rev. B **96**, 161201(R) (2017).

[39] P. G. Klemens, Proc. Phys. Soc. A **68**, 1113 (1955).

[40] S.-I. Tamura, Phys. Rev. B **27**, 858 (1983).

[41] F. Giazotto, T. T. Heikkilä, A. Luukanen, A. M. Savin, and J. P. Pekola, Rev. Mod. Phys. **78**, 217 (2006).

[42] P. E. Hopkins and J. R. Serrano, Phys. Rev. B **80**, 201408(R) (2009).